AIAA JOURNAL
Vol. 30, No. 4, April 1992

Helical-Perturbation Device for Cylinder-Wing Vortex Generators

Promode R. Bandyopadhyay,* John E. Riester,† and Robert L. Ash‡
NASA Langley Research Center, Hampton, Virginia 23665

A new device has been developed for introducing helical perturbations by means of low-level fluid injection into the cylinder boundary layer of a flow-aligned cylinder-wing vortex generator. Its basic characteristics have been analyzed and experimentally evaluated at moderate Reynolds numbers. When the cylinder boundary layer is tripped and there is no strong swirl, then in the near wake, the device lowers the mean rate of drop of the Strouhal number with Reynolds number by one-half. In the nearly nonexpanding and swirling far wake, both signs of input perturbations, namely co- and counter-rotating with the vortex, are detectable in the vortex core only confirming a wave-guide-like behavior. In the narrow frequency range of 80–100 Hz, these input perturbations slightly amplify downstream when counterrotating but attenuate in the corotating case.

Nomenclature

C = constant
c = airfoil chord
d = cylinder diameter (at the largest section, if applicable)
E = spectral (Figs. 3 and 7) or total (Figs. 8–10) energy of the axial velocity fluctuation
E_m = spectral axial energy of n
e = energy of axial velocity fluctuation within a specified narrow band centered at M_f
f = frequency, Hz
K = constant of proportionality characteristic of the device [Eq. (5)]
l = equivalent viscous length through gap
M_f = device rotational frequency, Hz
m = drop rate of St with Re [Eq. (8)]
n = dominant frequency, Hz
$\dot{Q}$ = incoming main stream flow rate per second
$\dot{q}$ = device air injection rate, l/s
Re = cylinder Reynolds number, $U_\infty d/\nu$
r = radial distance from cylinder axis
St = cylinder Strouhal number, nd/U_∞
St_m = device motor Strouhal number, $M_f d/U_\infty$
U_∞ = freestream velocity
V = injection velocity in the radial direction
V_m = mean injection velocity
v = fluctuating part of V
x = axial distance from the tail end of the cylinder
ΔP = device plenum pressure referenced to local wall static pressure in the incoming freestream
δ = injection gap created by the obliquely truncated disk
δ_0 = half of the maximum value of δ
η = transverse distance from injection midplane
θ = azimuthal angle (phase) of rotating disk
μ = dynamic viscosity
ν = kinematic viscosity
σ = standard of deviation

Introduction

PHENOMENA such as vortex bursting or the stability of aircraft trailing vortices are of considerable practical importance to mixing and flight safety. Although no general necessary and sufficient conditions for vortex stability[1] exist, the dominant majority of instabilities measured[2] and predicted[3–6] for unconfined trailing-line vortices are helical wave instabilities that depend on the direction of rotation of the helix. Axisymmetric modes can also be simultaneously present.[2] In shear flows like pipe flows,[7] jets,[8] and wakes and vortices,[9–11] helical disturbances are also believed to cause the laminar flow breakdown, or cause the quasiperiodic breakdown of the mean flow after the critical Reynolds number has been reached. However, few experiments have examined the behavior of controlled-input, helical disturbances in these flows.

The present experiment was started with a desire to control or trigger a bursting in a trailing-line vortex. In this paper, a new helical perturbation-generating device, designed to control swirling turbulent flows, and its fluid dynamic performance are described. The basic characteristics of this device are analyzed and experimentally verified using a flow-aligned cylinder-wing vortex generator, in two low-speed airflow facilities at NASA Langley Research Center. In the first experiment, which was conducted in the entry region of a pipe flow apparatus, the near-wake flow in the absence of any strong swirl is considered. In the second experiment, which was conducted in the long test section of a wind tunnel, the far wake with a strong swirl is examined; this nonexpanding wake has a trailing vortex-like characteristic.[12]

Device for Introducing Helical Perturbations

Description

A vortex generator, which is essentially a flow-aligned cylinder attached to a pair of matched airfoils, is described in Ref. 12. The present perturbation-generating device has been designed to be housed in this cylinder. Figure 1a shows a sketch of the device in the cylinder-wing assembly.[13] Two geometrically similar models have been evaluated. In the pipe and

Presented as Paper 90-1627 at the AIAA 21st Fluid Dynamics, Plasma Dynamics, and Lasers Conference, Seattle, WA, June 18–20, 1990; received Feb. 15, 1991; revision received July 26, 1991; accepted for publication Aug. 5, 1991.

*Adjunct Professor and Senior Research Associate, Mechanical Engineering and Mechanics Department, Old Dominion University, Hampton, VA; currently at Code 804, NUWC Division, Newport, RI, 02841. Associate Fellow AIAA.

†Research Associate, Mechanical Engineering and Mechanics Department, Old Dominion University, Norfolk, VA.

‡Professor and Chairman, Mechanical Engineering and Mechanics Department, Old Dominion University, Norfolk, VA. Associate Fellow AIAA.

wind-tunnel experiments, respectively, the models have the following dimensions: cylinder diameter 3.048 and 2.54 cm; airfoil chord c 6.35 and 10.16 cm; nominal airfoil angle of attack 0 and $\pm$ 8 deg; nose 3:1 ellipsoid in both pipe and wind tunnel; nose-to-airfoil leading-edge distance 7.94 and 16.83 cm; and nose-to-tail length 25.8 and 45.7 cm.

The device was driven by a dc motor mounted inside a hollow cylinder. Compressed air was plumbed through one of the airfoils into the hollow cylinder which was grooved to carry the air around the motor and into a plenum chamber. The cylindrical section contained a thrust bearing for the shaft which was connected to the motor by a small piece of plastic tubing. The shaft was supported by a second bearing that was mounted in a streamlined tail. Experiments with a different apparatus showed that the flow from a pipe impinging on a flat obstruction is viscosity-dominated when the gap is less than 0.2 mm. A viscosity-dominated flow through such a narrow gap could be used to produce a controlled velocity perturbation whereas a larger gap would produce an excessive mass flow perturbation. A rotating disk section was mounted on the shaft, which was machined as an obliquely truncated cylinder so that the disk was thinner by 0.2 mm on one edge (at $\theta = 0$ deg say) compared to that at the diametrically opposite edge ($\theta = 180$ deg) (Fig 1a, inset). The disk rotated beneath the slot, which was formed when the tail section was mated with the cylinder section (Fig. 1b). When the motor was positioned properly, the rotating disk blocked the slot (at $\theta = 180$ deg) on one side and provided a 0.2-mm gap on the opposite side of the slot. The plenum was located between the motor and the disk. Pressure differences $\mathcal{O}(1$ Torr) were required to produce injection velocities that were in the range of desired perturbation velocities [$\leq (0.1U_\infty)$]. The motor was capable of rotating the disk at speeds up to 300 Hz in either direction.

In the wind-tunnel experiments, the device had to be retrofitted to the pre-existing model where the cylinder diameter was 2.54 cm. A suitable motor small enough to fit within the cylinder, while leaving enough clearance for air passage and instrumentation, was not readily available, and so a slightly larger motor was used. Consequently, the outside diameter of the aluminum cylinder was raised to 3.048 cm in the region where the motor was housed to accommodate this larger motor. However, in the pipe experiment, the entire cylinder diameter was of diameter 3.048 cm. The (motor) wedge rotational speed was monitored by analyzing the spectrum of the dc motor commutator currents.

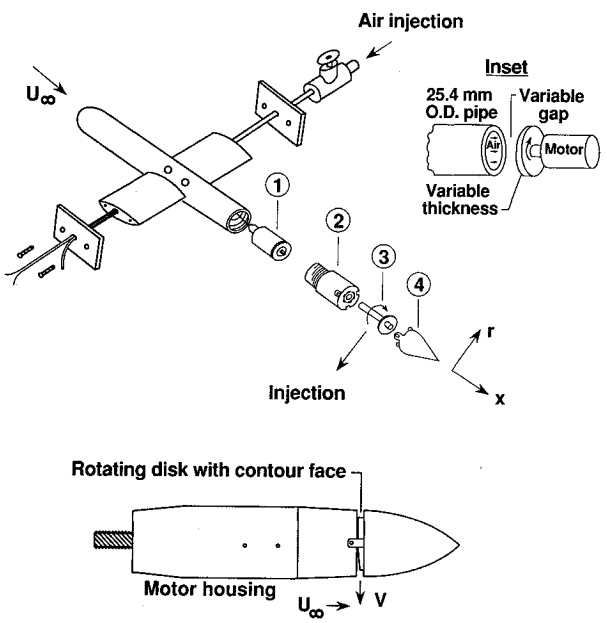

Fig. 1 Perturbation-generating device in the cylinder-wing vortex generator. a) 1: dc motor; 2: motor housing; 3: shaft with tapered disk; and 4: tail. Inset shows variable gap schematically. b) Device assembly showing disk inside slot.

Experimental Qualification of the Device

For reasons of availability, the basic performance of the device was experimentally determined in the entry region of a 10.2-cm-diam, 6-m-long acrylic plastic pipe flow facility.[14] Screens at the inlet and a rounded entry profile were used to control the freestream turbulence level which was about 0.05% at the model location at 5 m/s. A circular ring of small-diameter wire was glued to the cylinder nose near the point of stagnation to fix the transition location at lower Reynolds numbers and to help produce an axisymmetric laminar flow by locking the point of stagnation. A blower driven by a variable speed, 20-hp electric motor was used to draw air through the pipe and produce mean pipe flow velocities between 1.2 and 32 m/s. A smaller dc powered fan was substituted to produce lower speeds. Reference freestream velocity was measured using a pitot tube in combination with a local wall static tube, and boundary-layer velocity measurements were made using a linearized, single hot-wire anemometer. Local static and dynamic pressures were measured using miniature pitot probes and wall pressure taps, with electronic capacitive pressure gauges. A computer-controlled traverse was used to position the hot-wire probes vertically inside the pipe. Position could be measured within 10 μm in the vertical direction. The data acquisition and spectral analysis were carried out with a digital oscilloscope/waveform analyzer.

The perturbation signature quality M_f was investigated over a wide range of device frequencies M, plenum pressures (ΔP, referenced to local wall static pressure in the uniform stream), and incoming freestream velocities U_∞. Figure 2 shows a typical hot-wire velocity perturbation signature in the absence of any incoming uniform flow (i.e., $U_\infty = 0$). The device generated reasonable sinusoidal perturbations at low ΔP values. At high ΔP values [$\mathcal{O}$(46 Pa)], the perturbation was not purely sinusoidal, but the device nevertheless introduced one dominant frequency and weaker harmonics. Figure 3 shows that over a range of incoming uniform flow speeds, the device introduced a nearly monochromatic perturbation. The figure shows typical spectra for record lengths of 4.096 s sampled at 1 kHz.

Basic Characteristics of the Device

Analysis

The characteristic of the device is a function of Re, St_m, and ΔP. First, consider the device operating in the absence of any incoming uniform flow. The volume flow rate of injected air can be estimated by assuming that the flow is laminar. Then, since the gap varies with motor shaft phase θ, the injection gap $\delta(\theta)$ is given by

$$\delta(\theta) = \delta_0[1 + \cos\theta] \tag{1}$$

The velocity profile leaving the gap can be shown to be

$$V(\eta) = (3/2)V_m(\theta)[1 - \eta^2/\delta^2(\theta)] \tag{2}$$

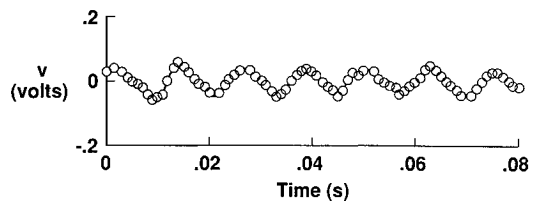

Fig. 2 Typical radial velocity perturbation signature above the device slot in the absence of incoming uniform flow in the pipe flow facility ($M_f = 80$ Hz, $\Delta P = 10$ Pa).

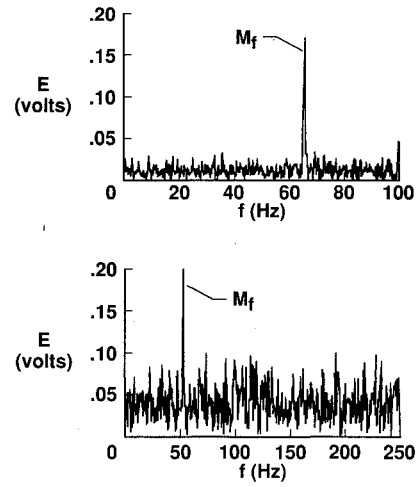

Fig. 3 Typical energy spectra of axial velocity fluctuation behind device ($x/d = 1.25$, $r/d = 0.5$) with uniform incoming flow in the pipe flow facility: a) $M_f = 66.4$ Hz, $U_\infty = 6.7$ m/s, $\Delta P = 14$ Pa; b) $M_f = 54.7$ Hz, $U_\infty = 25.5$ m/s, $\Delta P = 19$ Pa.

where η is a coordinate which is referenced to the midplane in the gap $-\delta_0 \leq \eta \leq \delta_0$, and $V_m(\theta)$ is the mean velocity at shaft phase θ, given by

$$V_m(\theta) = [\Delta P\, \delta^2(\theta)/3\mu l] \tag{3}$$

where μ is the dynamic viscosity and l is the equivalent viscous length traversed by the air through the gap. Using Eqs. (1-3), the estimated volumetric injection per rotation is given by

$$\frac{d}{2}\int_0^{2\pi} \delta(\theta) V_m(\theta)\, d\theta = \frac{5\pi d \Delta P}{6\mu l}\delta_0^3 \tag{4}$$

The volumetric injection per rotation per second $\dot{q}$ is then given by, if $\dot{q}$ is in liters per second and d and δ_0 are in millimeters,

$$\dot{q} = K\Delta P M_f \qquad \text{and} \qquad V_{\max} = (764/d\delta_0)K\Delta P \tag{5}$$

where the constant K can be determined experimentally and $V_{\max}$ is the maximum velocity in meters per second at the centerplane of the gap at $\theta = 0$.

The incoming main stream flow rate is expressed by $\dot{Q} = CU_\infty$, where C is a constant, and the injection ratio is given by

$$\dot{q}/\dot{Q} = \text{const}\ (M_f \Delta P/U_\infty) \tag{6}$$

Determination of Optimum Injection Ratio

Measurements were made with Re, St_m, and ΔP varying over two decades each, and M_f varying by a factor of more than 2. In these experiments, the energy spectrum of the axial velocity fluctuation at $x/d = 1.25$ and $r/d = 0.5$ was monitored while varying ΔP and M_f at a given U_∞. The values of ΔP and M_f that resulted in the largest peak in the spectrum at M_f were thus determined. The flow could be considered to be the most responsive to the input perturbations at these values of the variables. At this state, the device was said to be operating at an optimized state. The experimental data are plotted in Fig. 4 in terms of the injection ratio given in Eq. (6). At least over a decade of Re, the optimized response of the fluid dynamic system has taken place at a nearly constant injection ratio.

The maximum value of ΔP was less than 100 Pa in the pipe experiments. Based on the previous analysis, the injected volume flow rate was no more than 1% of the pipe flow volume flow rate. Measurements[13] of mean velocity profiles at $x/d = 1.25$ at $U_\infty = 6$ and 14 m/s with the device turned off or

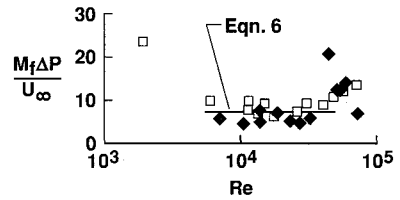

Fig. 4 Near constancy of injection ratio for optimized operation of control device in the pipe flow facility. Device: corotating (□) and counter-rotating (◆).

on at $M_f = 75$ Hz showed that momentum changes in the wake were less than 0.1%. These estimates indicate that the device introduced primarily a velocity and not a mass flow perturbation. The maximum velocity perturbation was about 5–10% of the incoming uniform flow.

Near-Wake Experiments with the Device: *St* vs *Re*

The effect of the device on the dominant perturbations in the near wake of the cylinder-wing combination was studied with energy spectra. For the spectra, the time length of the velocity records was 4.096 s and the sampling interval was 0.2 ms. With the injection cavity closed (that is, the device being turned off) at $x/d = 1.25$, the most dominant frequency whose energy is E_m reached the highest level at $r/d = 0.5$ both above and below the centerline, the airfoils being mounted horizontally. This indicated that the cylinder-wing combination was flow-aligned. The near-wake spectral results pertain to this location.

The upstream effects can be classified into two groups: 1) passive, with trip wire and open cavity (device being turned off) and 2) active, with the device turned on. The former results are given elsewhere.[13] The effects of turning the device on and off in a tripped boundary layer are given here. The length and velocity scales of a dominant frequency n are d and U_∞, respectively, and the Strouhal number is given by

$$St = nd/U_\infty \tag{7}$$

In a given spectrum, the spike at M_f is ignored in the determination of $n(\neq M_f)$. At the most dominant peak, the energy E is denoted by E_m. The values of St for which the peaks are above a threshold, namely, $E/E_m = 0.9$ and 0.8 have also been examined.

When the device is off, the St-Re data for $Re < 70 \times 10^3$ indicates a linear relationship:

$$St = m\, Re + St_0 \tag{8}$$

Since the input perturbation is weak, the basic form of Eq. (8) should not alter when the device is turned on. [Equation (8), of course, may not apply when $Re >> 70 \times 10^3$.] From least-square data fit to Eq. (8), it has been determined that for $E/E_m = 1.0$, the values of $-m \times 10^6$ and St_0, respectively, are (2.92, 0.233) when the device is off and (1.216, 0.238) when the device is on. Similarly, when $E/E_m = 0.9$ and 0.8, the values are (3.24, 0.248) and (2.77, 0.252), respectively, when the device is off and (1.365, 0.264) and (1.526, 0.270), respectively, when the device is on. The absolute values of the slope are lower when the device is on, irrespective of E/E_m. The St-Re data for the tripped and $E/E_m = 0.8$ case are shown in Figs. 5 and 6 for the device off and on modes, respectively. Typical ranges of $\pm\sigma$ in St data at a given Re are indicated by vertical bars in the figures and the symbols denote the mean values. In Fig. 5, all data are within $\pm 20\%$ of the mean line whereas 80% of the population is within that range in Fig. 6. The scatter in the St data about the mean line and the σ value in each data point are slightly larger (but random and symmetric), when the device is turned on, due to unavoidable vibration. Figures 5 and 6 show that, when the cylinder boundary

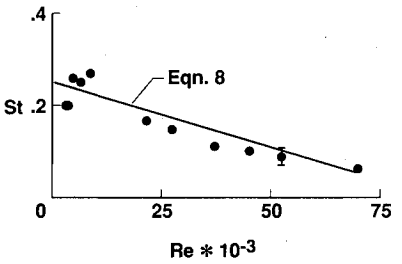

Fig. 5 Strouhal number vs Reynolds number variation in the near wake in the pipe flow facility. Device: off.

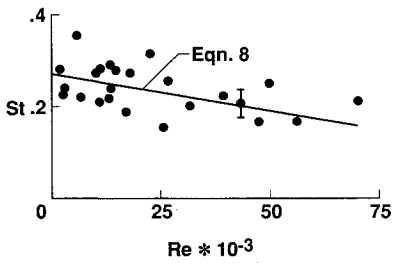

Fig. 6 Strouhal number vs Reynolds number variation in the near wake in the pipe flow facility. Device: on.

layer is tripped, the device can reduce the drop in the mean evel of *St* in the *Re* range investigated. It is suspected that the device is controlling the large turbulence structures.

A Strouhal number of roughly 0.2 in flat-plate wakes (where d = plate thickness) is well known. It is known that Tollmien-Schlichting (TS) waves whose origins are in the transitional phase are amplified and persist at higher Reynolds number even after passage over embedded cavities.[15] Here, it is suggested that a TS-wave-like ring mode is persisting in the cylinder boundary layer beyond transition to higher Reynolds numbers and the device is exciting these structures. The physical mechanism might be similar to that in the controlled acoustic excitation of a round jet, which can suppress turbulence by decreasing the spatial growth rate of energy containing eddies.[16-17] This needs a further study.

Far-Wake Experiments with the Device

The far-wake experiments were carried out in the NASA Langley 2- × 3-ft closed-circuit boundary-layer channel. The test section was 0.91 m wide, 0.61 m high, and 6.1 m long. Maximum speed was 50 m/s, the freestream turbulence being 0.03% at the model location.[12] The longer vortex generator was installed in this tunnel but this time the angle of attack of the airfoils was increased from 0 to 8 deg. The angle of attack was positive in one airfoil and negative in the other so as to create a strong swirl. Here, the device rotation is described as co- or counter-rotating in reference to the circumferential rotation of the vortex. Detailed seven-hole probe and x-wire measurements of the three components of the mean velocity and second- and third-order turbulence moments in the far field (x/c = 40) (in absence of the device) are reported in Ref. 12. The axial velocity profile was wake-like and the shear layer was practically nonexpanding. The circumferential velocity profile was linear over radial distances of the order of the cylinder diameter. As in the near-wake experiments in the pipe, the device was installed downstream of the airfoil. Measurements were carried out across the vortex at x/x = 17 and 40 at U_∞ = 13.7, 21, and 42 m/s and M_f varying from 45 to 180 Hz.

Figure 7 shows typical spectra across the vortex for the counter-rotating device. The spectral peak at the perturbation frequency (M_f) is clear only in the core. This confirms a wave-guide-like behavior of the core as has been proposed by Leibovich.[3]

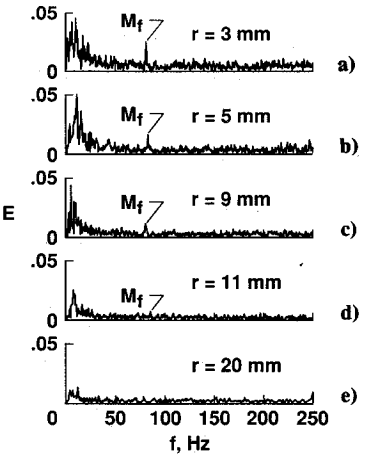

Fig. 7 Energy spectra in the far wake with strong swirl for counter-rotating control perturbation (x/c = 40, U_∞ = 13.7 m/s, M_f = 79–84 Hz, ΔP = 175–200 Pa).

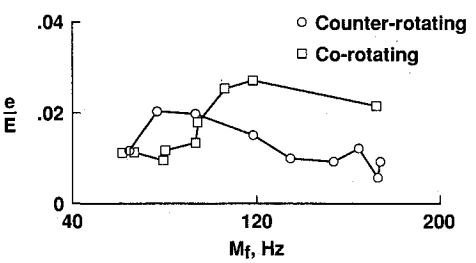

Fig. 8 Comparison of co- and counter-rotating perturbation energy levels in the far-wake core with strong swirl (x/c = 17, U_∞ = 42 m/s, frequency band = $M_f \pm 2$ Hz).

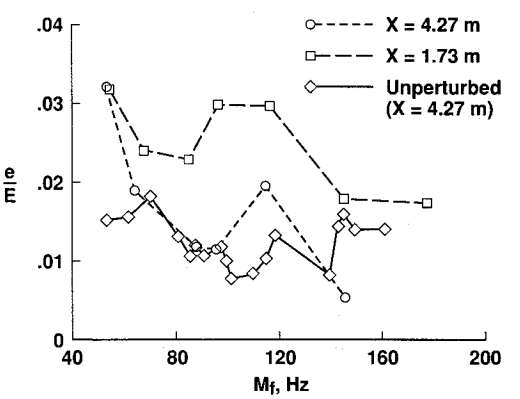

Fig. 9 Streamwise variation of energy levels for corotating perturbations in the far-wake core with strong swirl (r/d = 0, U_∞ = 13.7 m/s, frequency band = $M_f \pm 2$ Hz).

Energy levels (e) in the wake in narrow frequency bands, namely, $M_f \pm 0.5$ Hz, ± 1.0 Hz, and ± 2.0 Hz, were measured across the vortex for the co- and counter-rotating device, and the typical results at r = 0 for the band $M \pm 2.0$ Hz are compared in Fig. 8. The levels are nondimensionalized by E, the total energy over the entire spectrum. Velocity record lengths were 20.48 s. Interestingly, in the range 80 Hz > M_f > 100 Hz, energy is higher in the counter-rotating input mode. Computations show that, in some situations, counter-rotating disturbances, in fact, amplify more.[4]

The streamwise attenuation/amplification of the energy at M_f is shown in Figs. 9 and 10 for the co- and counter-rotating modes, respectively. The energy level in the narrow frequency band in the unperturbed case at the downstream station is also included for reference. Interestingly, in the range 80 Hz > M_f > 100 Hz, the counter-rotating input mode shows a slight

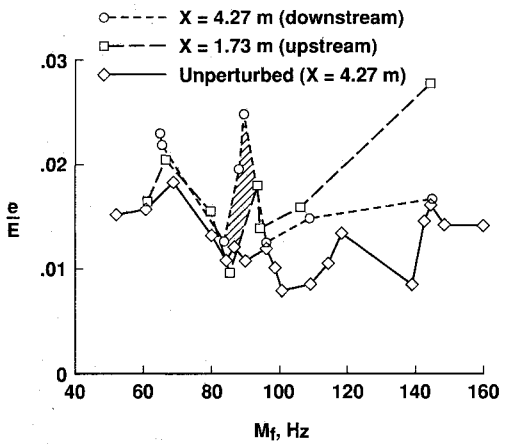

Fig. 10 Streamwise variation of energy levels for counter-rotating perturbations in the far-wake core with strong swirl ($r/d = 0$, $U_\infty = 13.7$ m/s, frequency band $= M_f \pm 2$ Hz). Hatched area shows downstream amplification.

amplification and the corotating mode shows an attenuation. This result might be of significance to stability.[4]

The effects of the co- and counter-rotating input modes on the mean velocity and turbulence profiles across the vortex are given in Ref. 13. Since there is no generic trailing vortex, there is a need to evaluate the vortex bursting performance of the device in other types of vortices, notably in low drag wing tip vortices that have a jet-type axial velocity profile.[18]

Conclusions

A new axisymmetric device for introducing helical perturbations into the boundary layer of a flow-aligned cylinder-wing vortex generator has been developed and evaluated. The theoretical condition for constant injection ratio has been derived and measured for maximum flow response. In the range $Re < 10^5$, when the cylinder boundary layer is tripped and in the near-wake flow in the absence of any strong swirl, the device slows down the mean drop rate in the Strouhal number of the dominant perturbations with Reynolds number by one-half. In the far wake in the presence of a strong swirl, the input helical perturbations survive only in the vortex core indicating a wave-guide-like behavior. In the far-wake core, in the frequency range of 80–100 Hz, the input perturbation remains more energetic and slightly amplifies downstream in the counter-rotating mode, whereas it is less energetic and attenuates downstream in the corotating mode.

Acknowledgment

The support of NASA (PRB: NAS1-18599; JER and RLA: NAG1-530) is acknowledged.

References

[1]Howard, L. N., and Gupta, A. S., "On the Hydrodynamic and Hydromagnetic Stability of Swirling Flows," *Journal of Fluid Mechanics*, Vol. 14, 1962, pp. 463–467.

[2]Singh, P. I., and Uberoi, M., "Experiments on Vortex Stability," *Physics of Fluids*, Vol. 19, No. 12, 1976, pp. 1858–1863.

[3]Leibovich, S., "Vortex Stability and Breakdown: Survey and Extension," *AIAA Journal*, Vol. 22, No. 10, 1984, pp. 1192–1206.

[4]Khorrami, M. R., "A Study of the Temporal Stability of Multiple Cell Vortices," Ph.D. Dissertation, Mechanical Engineering and Mechanics Dept., Old Dominion Univ., Norfolk, VA, May 1989.

[5]Lessen, M., and Paillet, F., "The Stability of a Trailing Line Vortex: Part 2, Viscous Theory," *Journal of Fluid Mechanics*, Vol. 65, 1974, pp. 769–779.

[6]Lessen, M., Singh, P. J., and Paillet, F., "The Stability of a Trailing Line Vortex: Part 1, Inviscid Theory," *Journal of Fluid Mechanics*, Vol. 63, 1974, pp. 753–763.

[7]Bandyopadhyay, P. R., "Aspects of the Equilibrium Puff in Transitional Pipe Flow," *Journal of Fluid Mechanics*, Vol. 163, 1986, pp. 439–458.

[8]Tso, J., and Hussain, F., "Organized Motions in a Fully Developed Turbulent Axisymmetric Jet," *Journal of Fluid Mechanics*, Vol. 203, 1989, pp. 425–448.

[9]Fiedler, H., "Coherent Structures in Turbulent Flows," *Progress in Aeronautical Science*, Vol. 25, 1988, pp. 231–269.

[10]Sarpkaya, T., "On Stationary and Traveling Vortex Breakdown," *Journal of Fluid Mechanics*, Vol. 45, 1971, pp. 545–559.

[11]Sarpkaya, T., "Effect of Adverse Pressure Gradient on Vortex Breakdown," *AIAA Journal*, Vol. 12, 1974, pp. 602–607.

[12]Bandyopadhyay, P. R., Stead, D. J., and Ash, R. L., "The Organized Nature of a Turbulent Trailing Vortex," *AIAA Journal*, Vol. 29, No. 10, 1991, pp. 1627–1633.

[13]Riester, J. E., "Development of a Perturbation Generator for Vortex Stability Studies," M.S. Thesis, Mechanical Engineering and Mechanics Dept., Old Dominion Univ., Hampton, VA, 1990.

[14]Bandyopadhyay, P. R., and Weinstein, L. M., "A Reflection-Type Oil-Film Skin-Friction Meter," *Experiments in Fluids*, Vol. 11, No. 5, 1991, pp. 281–292.

[15]Bandyopadhyay, P. R., "Resonant Flow in Small Cavities Submerged in a Boundary Layer," *Proceedings of the Royal Society of London*, Series A, Vol. 420, No. 1859, 1988, pp. 219–245.

[16]Crow, S. C., and Champagne, F. H., "Orderly Structure in Jet Turbulence," *Journal of Fluid Mechanics*, Vol. 48, 1971, pp. 547–591.

[17]Kudryashov, A. V., Mansfel'd, A. D., Rabinovich, M. I., and Suschik, M. M., "Modulation Mechanism of Suppression of Turbulence in Shear Flows," *Soviet Physics—Doklady*, Vol. 29, No. 7, 1984, pp. 530–532.

[18]Stifle, K. E., and Panton, R. L., "Experiments Concerning the Theories of Vortex Breakdown," AIAA 29th Aerospace Science Meeting, Paper 91-0736, Reno, NV, Jan. 1991.